

Influence of viscous dissipation on the exiting sheet thickness in the calendaring of Newtonian fluids

José C. Arcos
ESIME UA

Instituto Politécnico Nacional
México D.F., 02250

Email: <http://www.ipn.mx>

Oscar E. Bautista
ESIME UA

Instituto Politécnico Nacional
México D.F., 02250

Email: obautista@ipn.mx

Federico Méndez
Facultad de Ingeniería
UNAM

México D.F., 04510

Email: fmendez@unam.mx

Juan P. Escandón
ESIME UA

Instituto Politécnico Nacional
México D.F., 02250

Email: jescandon@ipn.mx

Abstract—In this work we treat theoretically the calendaring process of Newtonian fluids with finite *sheet* initial thickness, taking into account that the viscosity of the fluid is a well-defined function of the temperature. We predict the influence of the temperature-dependent viscosity on the exiting sheet thickness in the calendaring process. The mass, momentum and energy balance equations, based on the lubrication theory, were nondimensionalized and solved for the velocity, pressure and temperature fields by using perturbation and numerical techniques, where the exiting sheet thickness represents an eigenvalue of the mathematical problem. The numerical results show that the inclusion of temperature-dependent viscosity effect reduces about 20% the leave-off distance in comparison with the case of temperature-independent viscosity.

I. INTRODUCTION

The specialized literature for the calendaring process is reviewed in the following paragraphs. The theoretical analysis regarding the above mechanism was developed by Gaskell [1] and McKelvey [2] for isothermal Newtonian fluid. Zheng and Tanner [?] applied the Phan-Thien-Tanner fluid model for the calendaring process of inelastic and viscoelastic sheets using a perturbation method. Mitsoulis [3] numerically investigated the shape of the free surfaces of the entering and exiting sheets for the process of calendaring viscoplastic sheets with a finite thickness. The combined effects of asymmetry and viscous heating for the non-isothermal nip flow in calendaring were considered by Dobbels and Mewis [4]. The effect of viscous dissipation on calendaring process of Newtonian and power-law fluids have been studied by Kiparissides and Vlachopoulos [5]. They reported the temperature profiles due to viscous dissipation in calendaring gap, finding two maxima in the vicinity of the roll surfaces. In addition, the maximum temperatures exhibit two local maxima and one minimum in the direction of the flow. It appears that the only work about non-isothermal calendaring of Newtonian fluids is just the aforementioned work. However, in this work they determined the temperature profile, disregarding the influence of the temperature on the final exiting sheet thickness. In this direction, Middleman [6] developed a simple model of the sensitivity of calendered thickness to temperature fluctuations. He concluded that "a 3° variation in temperature will cause more than 20 percent variation in calendered thickness!". In this sense, to our knowledge there are not works that validate the aforementioned sentence. Therefore, the goal of this work is to determine the influence of the viscous dissipation on the dimensionless

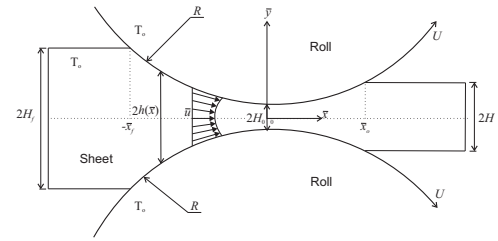


Fig. 1. Schematic diagram of the studied physical model, in physical variables.

exiting sheet thickness for the calendaring process taking into account the temperature-dependent viscosity .

A. Formulation

In Fig. 1, we show a sketch of the studied physical model. Two cylinders separated by a thin film of a Newtonian liquid with temperature dependent viscosity, are rotated in the same direction. Each cylinder has a radius R , rotating with a constant angular velocity, ω , resulting in a linear velocity at its surface given by $U = \omega R$. The minimum gap half-height, H_0 , is such that $H_0 \ll R$ and the one-half exiting sheet thickness is represented by H . The geometry of the roll surface is given as $h(\bar{x}) = H_0(1 + \bar{x}^2/2RH_0)$ [6]. We assume that the roll surfaces are found at a constant temperature, T_0 . The location \bar{x} where the sheet first bites the rolls is represented by $-\bar{x}_f$, which is known. On the other hand, the leave-off distance location of the sheet, modified by temperature effects, represented by λ is unknown, and must be determined in the present analysis. The mass, momentum and energy equations, in steady state, are the following

$$\frac{\partial \bar{u}}{\partial \bar{x}} + \frac{\partial \bar{v}}{\partial \bar{y}} = 0 \quad , \quad (1)$$

$$\rho \bar{u} \frac{\partial \bar{u}}{\partial \bar{x}} + \rho \bar{v} \frac{\partial \bar{u}}{\partial \bar{y}} = -\frac{\partial \bar{P}}{\partial \bar{x}} + \frac{\partial \bar{\tau}_{yx}}{\partial \bar{y}} \quad , \quad (2)$$

$$\rho \bar{u} \frac{\partial \bar{v}}{\partial \bar{x}} + \rho \bar{v} \frac{\partial \bar{v}}{\partial \bar{y}} = -\frac{\partial \bar{P}}{\partial \bar{y}} + \frac{\partial \bar{\tau}_{xy}}{\partial \bar{x}} \quad , \quad (3)$$

$$\rho c_p \bar{u} \frac{\partial T}{\partial \bar{x}} = k \left(\frac{\partial^2 T}{\partial \bar{x}^2} + \frac{\partial^2 T}{\partial \bar{y}^2} \right) + \bar{\tau}_{xy} \frac{\partial \bar{u}}{\partial \bar{y}} \quad ; \quad (4)$$

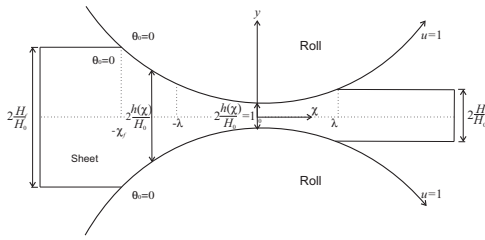


Fig. 2. Schematic diagram of the studied physical model, in dimensionless variables.

where the shear stress is given as [7],

$$\bar{\tau}_{xy} = \bar{\tau}_{yx} = \mu_0 \exp[-a(T - T_0)] \left(\frac{\partial \bar{u}}{\partial \bar{y}} + \frac{\partial \bar{v}}{\partial \bar{x}} \right) \quad (5)$$

The boundary and initial conditions associated with Eqs. (1)-(4) are

$$\bar{y} = 0 : \frac{\partial \bar{u}}{\partial \bar{y}} = 0 \quad , \quad (6)$$

$$\bar{y} = h(\bar{x}) : \bar{u} = U \quad , \quad (7)$$

$$\bar{y} = 0 : \frac{\partial T}{\partial \bar{y}} = 0 \quad , \quad (8)$$

$$\bar{y} = h(\bar{x}) : T = T_0 \quad , \quad (9)$$

$$\bar{x} = -\bar{x}_f : T = T_0 \quad . \quad (10)$$

In the region of the nip and extending to either side (i. e., in the $\pm \bar{x}$ direction) by a distance of the order of \bar{x}_0 (see Fig. 1), the roll surface are nearly parallel when $H_0 \ll R$. Then, we can assume that the flow is nearly parallel, so that $\bar{v} \ll \bar{u}$ and $\frac{\partial}{\partial \bar{x}} \ll \frac{\partial}{\partial \bar{y}}$, as we will show below. According to this assumption, the boundary conditions (6-10) are those used in the lubrication approximation theory.

In the above equations, \bar{u} , \bar{v} , \bar{P} and T represent the velocity components in \bar{x} and \bar{y} directions, pressure and temperature fields of the fluid, respectively. ρ , c_p , k , μ_0 are the density, specific heat, thermal conductivity and the viscosity of the Newtonian liquid evaluated at a reference temperature T_0 , respectively. In addition, a is an empirical parameter that measures the dependence of the viscosity on the temperature; this constant is of order of 10^{-2} to 10^{-1} [6, 7]. In Eq. (5) we have included the exponential temperature dependence model for the viscosity [7].

1) *Dimensionless Equations:* In this section, we present the dimensionless governing equations needed to solve the non-isothermal calendering process, Fig. 2. Based on the order of magnitude analysis carried out previously, we can define the following dimensionless variables

$$\chi = \frac{\bar{x}}{\sqrt{2RH_0}}, \quad y = \frac{\bar{y}}{H_0}, \quad \frac{h(\bar{x})}{H_0} = 1 + \chi^2 \quad (11)$$

$$P = \frac{\bar{P}H_0}{\mu_0 U}, \quad \lambda^2 = \frac{H}{H_0} - 1, \quad Q(\chi) = \frac{\bar{Q}}{2UH_0}$$

$$u(\chi, y) = \frac{\bar{u}(\bar{x}, \bar{y})}{U}, \quad v(\chi, y) = \frac{\bar{v}(\bar{x}, \bar{y})\sqrt{2RH_0}}{UH_0}$$

$$\theta(\chi, y) = \sqrt{\frac{H_0}{2R}} \frac{(T(\bar{x}, \bar{y}) - T_0)\rho_f c_p H_0}{\mu_0 U}$$

Introducing the dimensionless variables defined by previous relationships (11) into the conservation equations (1)-(5), we obtain

$$Re\beta \left(u \frac{\partial u}{\partial \chi} + v \frac{\partial u}{\partial y} \right) = -\beta \frac{dP}{d\chi} + \frac{\partial}{\partial y} \left(e^{-\epsilon\theta} \frac{\partial u}{\partial y} \right), \quad (12)$$

$$Gz u \frac{\partial \theta}{\partial \chi} = \frac{\partial^2 \theta}{\partial y^2} + Gz e^{-\epsilon\theta} \left(\frac{\partial u}{\partial y} \right)^2 \quad . \quad (13)$$

Here, ϵ is a dimensionless parameter, given as $\epsilon = Na/Gz$, where Na is the Nahme-Griffith number [8, 9], defined as $Na = a(\mu_0 U^2/k)$, and Gz is the well-known Graetz number, given by $Gz = \beta Pe$. Here Pe is the Peclet number, represented by $Pe = (\rho c_p/k)UH_0$, and β is a geometric parameter, defined as $\beta = (H_0/2R)^{1/2}$. The Nahme-Griffith number represents the ratio of the temperature rise, due to viscous dissipation to the temperature rise needed to change the viscosity. Re is the Reynolds number, defined as $Re = \rho UH_0/\mu_0$. In typical applications of calendering, $\epsilon \ll 1$, in such a way that the exponential factor, in the momentum and energy equations, can be linearized as $e^{-\epsilon\theta} \approx 1 - \epsilon\theta + \dots$, and the Reynolds number is much less than unity, $Re \sim 10^{-4} - 10^{-5}$, indicating that the inertia plays a minor role in this process; the Peclet number takes values of order of 10^2 to 10^3 . According to the previous discussion, Eq. (12) transforms to

$$\beta \frac{dP}{d\chi} = \frac{\partial}{\partial y} \left[(1 - \epsilon\theta + \dots) \frac{\partial u}{\partial y} \right] \quad , \quad (14)$$

with the following dimensionless boundary conditions,

$$\frac{\partial u}{\partial y} \Big|_{y=0} = 0 \quad , \quad (15)$$

$$u(y = 1 + \chi^2) = 1 \quad . \quad (16)$$

Furthermore, Eq. (14) requires additional boundary conditions for the pressure gradient $dP/d\chi$ and the pressure P , given by

$$\frac{dP}{d\chi} \Big|_{\chi=\lambda} = P(\chi = \lambda) = 0 \quad , \quad (17)$$

$$P(\chi = -\chi_f) = 0 \quad . \quad (18)$$

On the other hand, the energy equation, Eq. (13), takes the form

$$Gz u \frac{\partial \theta}{\partial \chi} = \frac{\partial^2 \theta}{\partial y^2} + Gz (1 - \epsilon \theta + \dots) \left(\frac{\partial u}{\partial y} \right)^2, \quad (19)$$

with the boundary conditions,

$$\theta(-\chi_f, y) = 0, \quad (20)$$

$$\theta(\chi, 1 + \chi^2) = 0, \quad (21)$$

$$\left. \frac{\partial \theta}{\partial y} \right|_{y=0} = 0. \quad (22)$$

Together with Eqs. (14) and (19), we need the dimensionless mass balance equation, which can be written in the form,

$$Q = 1 + \lambda^2 = \int_0^{1+\chi^2} u \, dy, \quad (23)$$

where Q is the volumetric flow rate and for the present formulation, assumes a constant value. In addition, λ represents an unknown eigenvalue of the mathematical problem and is related to the exiting sheet thickness for the calendering process through the following relationship $\lambda^2 = H/H_0 - 1$. We anticipate that this parameter is directly influenced by temperature effects in contrast to those that do not consider the inclusion of these effects. The system of equations (14) and (19) represent the well known *lubrication approximation* [8] for a Newtonian liquid with temperature-dependent viscosity.

From the classical calendering analysis [1, 8], for Newtonian liquids, there are two flow regions in the x -direction: one region near to the entrance and other at the exit of the nip. These two regions have a positive pressure gradient in the domain $-\chi_f \leq \chi \leq -\lambda$ and a negative pressure gradient, in this other interval $-\lambda \leq \chi \leq \lambda$. In the following section and for each region, we obtain the corresponding velocity, pressure and temperature profiles.

B. Asymptotic solution for the limit $\epsilon \ll 1$.

To determine the dimensionless velocity, pressure, temperature profiles, leave-off distance and the corresponding exiting thickness of the calendered material, we conduct an asymptotic solution by decoupling the system of Eqs. (14) and (19). Applying a regular perturbation technique and using ϵ as the perturbation parameter, we propose the following expansions,

$$u(\chi, y) = u_0(\chi, y) + \epsilon u_1(\chi, y) + \dots, \quad (24)$$

$$P(\chi) = P_0(\chi) + \epsilon P_1(\chi) + \dots, \quad (25)$$

$$Q = Q_0 + \epsilon Q_1 + \dots, \quad (26)$$

$$\theta(\chi, y) = \theta_0(\chi, y) + \epsilon \theta_1(\chi, y) + \dots, \quad (27)$$

$$\lambda = \lambda_0 + \epsilon \lambda_1 + \dots, \quad (28)$$

where u_0, P_0, Q_0, λ_0 and θ_0 are the leading-order solutions for the isothermal case and solved in previous works [1, 2, 8]. P_1, Q_1, u_1, θ_1 and λ_1 are corrections up to terms of first-order. Introducing the relationships (24)-(28) into Eqs. (14)-(23), we obtain, after collecting terms of the same power of ϵ , the following sets of equations

for ϵ^0 :

$$\beta \frac{dP_0}{d\chi} = \frac{\partial^2 u_0}{\partial y^2}, \quad \text{for } -\chi_f \leq \chi \leq \lambda_0, \quad (29)$$

$$Q_0 = 1 + \lambda_0^2 = \int_0^{1+\chi^2} u_0 \, dy, \quad (30)$$

$$Gz u_0 \frac{\partial \theta_0}{\partial \chi} = \frac{\partial^2 \theta_0}{\partial y^2} + Gz \left(\frac{\partial u_0}{\partial y} \right)^2. \quad (31)$$

The boundary conditions for Eqs. (29)-(31) are:

$$\frac{\partial u_0}{\partial y} = 0 \quad \text{and} \quad \frac{\partial \theta_0}{\partial y} = 0, \quad \text{at } y = 0, \quad (32)$$

$$u_0 = 1 \quad \text{and} \quad \theta_0 = 0, \quad \text{at } y = 1 + \chi^2, \quad (33)$$

$$P_0 = 0 \quad \text{and} \quad \theta_0 = 0, \quad \text{at } \chi = -\chi_f, \quad (34)$$

$$\frac{dP_0}{d\chi} = P_0 = 0 \quad \text{at } \chi = \lambda_0. \quad (35)$$

For the first order solution, ϵ^1 :

$$\beta \frac{dP_1}{d\chi} = \frac{\partial u_1}{\partial y} - \theta_0 \frac{\partial u_0}{\partial y}, \quad \text{for } -\chi_f \leq \chi \leq \lambda_1, \quad (36)$$

$$Q_1 = 2\lambda_0\lambda_1 = \int_0^{1+\chi^2} u_1 \, dy. \quad (37)$$

For solving Eqs. (36) and (37), we need the zeroth-order solution for mass, momentum and energy equations, Eqs. (29)-(31). The boundary conditions for Eqs. (36) and (37) are written as,

$$\frac{\partial u_1}{\partial y} = 0 \quad \text{and} \quad \frac{\partial \theta_1}{\partial y} = 0, \quad \text{at } y = 0, \quad (38)$$

$$u_1 = 0 \quad \text{and} \quad \theta_1 = 0, \quad \text{at } y = 1 + \chi^2, \quad (39)$$

$$P_1 = 0 \quad \text{and} \quad \theta_1 = 0, \quad \text{at } \chi = -\chi_f, \quad (40)$$

$$\frac{dP_1}{d\chi} = P_1 = 0 \quad \text{at} \quad \chi = \lambda_1. \quad (41)$$

1) *Zeroth-order solution:* The solution of Eq.(29), considering a finite feed thickness, is given by:

$$u_0 = 1 + \frac{1}{2}\beta \left(\frac{dP_0}{d\chi} \right) \left[y^2 - (1 + \chi^2)^2 \right], \quad (42)$$

with

$$\frac{dP_0}{d\chi} = -3\beta^{-1} \frac{(\lambda_0^2 - \chi^2)}{(1 + \chi^2)^3}, \quad (43)$$

for $-\chi_f \leq \chi \leq \lambda_0$.

We must emphasize that the zeroth-order solution, Eqs. (42) and (43), were obtained in previous works [1, 8]. In the present analysis, the zeroth-order energy equation, Eq. (31), was solved in the two flow regions in the χ direction: one region near to the nip at the entrance to the rolls, which has a positive pressure gradient; and the other region away from the nip at the exit, with opposite sign for the pressure gradient.

Due to the curvature of the rolls, we use a simple independent variable transformation that makes possible to solve the dimensionless energy equation on a uniformly spaced computational grid, therefore we can introduce the following transformation variable, $Y = y / (1 + \chi^2)$, then Eq. (31) takes the form,

$$Gz u_0 \frac{\partial \theta_0}{\partial \chi} = \frac{1}{(1 + \chi^2)^2} \frac{\partial^2 \theta_0}{\partial Y^2} + Gz \left(\frac{1}{1 + \chi^2} \frac{\partial u_0}{\partial Y} \right)^2. \quad (44)$$

In the new independent variable, Y , the zeroth-order velocity profile is given by

$$u_0 = 1 + \frac{3}{2} \frac{(\chi^2 - \lambda_0^2)}{1 + \chi^2} (Y^2 - 1), \quad (45)$$

the boundary conditions, given by Eqs. (32) and (33), associated with the Eq. (44) are transformed to

$$Y = 0 : \frac{\partial \theta_0}{\partial Y} = 0, \quad (46)$$

$$Y = 1 : \theta_0 = 0. \quad (47)$$

Equation (44) was numerically solved by using the conventional Crank-Nicolson method. To solve this equation, we selected a mesh with 501 nodal points for the half width and 1027 in the direction of the flow. The details are omitted for simplicity.

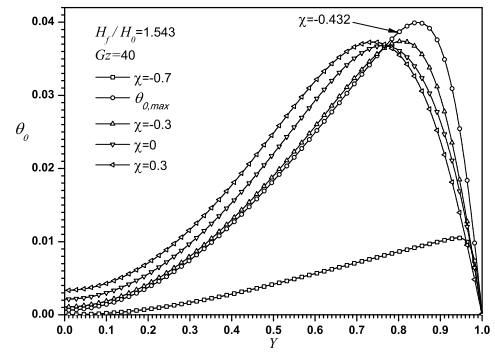


Fig. 3. Dimensionless temperature θ_0 as a function of the dimensionless longitudinal χ and transversal Y coordinates, $Gz = 40$, $H_f/H_0 = 1.543$, at five different positions of the variable χ

2) *First order solution:* The solution procedure for the first-order is similar to the zeroth-order solution; we begin integrating Eq. (36) to find u_1 explicitly as a function of Y , in terms of the independent variable transformation $y = (1 + \chi^2)Y$, after applying the boundary conditions (38) and (39) takes the form

$$u_1(\chi, Y) = \frac{1}{2}\beta (1 + \chi^2)^2 \frac{dP_1}{d\chi} [Y^2 - 1] - \beta (1 + \chi^2)^2 \frac{dP_0}{d\chi} \left[\int_0^1 \theta_0 Y dY - \int_0^Y \theta_0 Y dY \right]. \quad (48)$$

Replacing Eq. (48) into Eq. (37), and applying the boundary condition, given by Eq. (41) we obtained the volumetric flow rate for the first order and after some algebraic manipulations, we can also obtain one explicit expression for $dP_1/d\chi$

$$Q_1 = \frac{\left(-\frac{dP_0}{d\chi} \right)_{\chi=\lambda_1}}{(\beta^{-1} (1 + \lambda_1^2)^{-3})} \left\{ \begin{array}{l} \left[\int_0^1 \int_0^1 \theta_0 Y dY dY \right] \\ - \int_0^1 \int_0^Y \theta_0 Y dY dY \end{array} \right\} \quad (49)$$

$$\frac{dP_1}{d\chi} = \frac{9}{\beta} \left\{ \begin{array}{l} \frac{(\lambda_0^2 - \lambda_1^2)}{(1 + \chi^2)^3} \left[\int_0^1 \int_0^1 \theta_0 Y dY dY \right] \\ - \int_0^1 \int_0^Y \theta_0 Y dY dY \\ - \frac{(\lambda_0^2 - \lambda_1^2)}{(1 + \chi^2)^3} \left[\int_0^1 \int_0^1 \theta_0 Y dY dY \right] \\ - \int_0^1 \int_0^Y \theta_0 Y dY dY \Big|_{\chi=\lambda_1} \end{array} \right\} \quad (50)$$

2) This equation is valid for $-\chi_f \leq \chi \leq \lambda_1$, where λ_1 must be determined as a part of the problem. In the above equation, the procedure to evaluate the integral terms is the following: at each axial position, χ , the term given by the first integral, $\int_0^1 \int_0^1 \theta_0 Y dY dY$, is found numerically by using the Trapezoidal rule. Specifically, this procedure was implemented at each axial position, χ , from the point where the entering sheet first bites the rolls [8] to the leave-off distance point of the rolls, given by the zeroth order solution of λ_0 . For the obtained data in this numerical integration, one ninth-degree

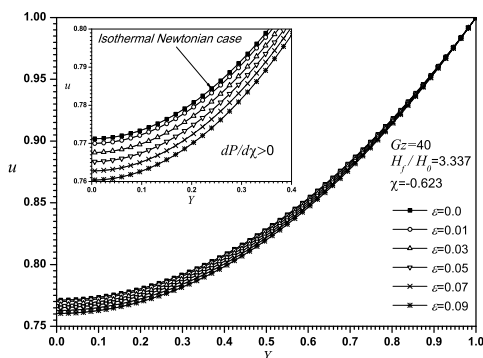


Fig. 4. Dimensionless velocity distribution u for different values of the parameter ϵ , as a function of the dimensionless transverse coordinate Y , evaluated at $\chi = -0.623$, for $H_f/H_0 = 3.337$ and $Gz = 40$.

polynomial regression was generated as a function of the axial coordinate χ .

For the second integral, $\int_0^1 \int_0^Y \theta_0 Y dY dY$, at each axial position, χ , we have obtained the data points, $(Y_j, \theta_{o,j} Y_j)$, where j represents the position for each transverse location and from which we can fit a ninth-degree polynomial for the Y coordinate. Once this is done, each resulting polynomial was integrated from $Y = 0$ to $Y = 1$ using the Trapezoid rule. We omit the presentation of these polynomials because approximately 1000 polynomials were generated.

3) In order to find the first order of the dimensionless flow rate, Q_1 , and consequently λ_1 , an iterative procedure was applied to Eq. (50). At the starting of the iterative procedure, we assume a value for λ_1 . Once this is done, the first order of dimensionless pressure $P_1(\chi)$ was obtained by integrating Eq. (50) using a conventional fourth-order Runge-Kutta technique. The procedure was repeated until the boundary condition given by Eq. (41) was fully satisfied.

II. RESULTS

For the numerical results presented in this section, we have used representative values of the parameters involved in the calendaring process [9, 10]. Figure 3 shows the numerical solution for the dimensionless temperature θ_0 as a function of the dimensionless transverse direction at five axial positions, χ , for two fixed different entering sheet thickness, $H_f/H_0 (=1.543, 3.337)$ and $Gz=40$, respectively. In these figures, we can note that the maximum values of the dimensionless temperature are confined to the vicinity of the roll surface for each χ position. These are the results of the interaction between the viscous dissipation of the fluid and the heat transfer mechanisms to the rolls. For the same figures, the larger values of the dimensionless temperature in the χ direction are located near to the entry.

In Figs. 4 and 5, the velocity profiles were evaluated in a position χ , which corresponds to the region where pressure gradient has a positive value, and the other region with opposite sign. From these figures, we can see that the dimensionless velocity u decreases as the parameter ϵ increases. This decrease on the dimensionless velocity is insignificant in the vicinity of the rolls and more pronounced at the center plane.

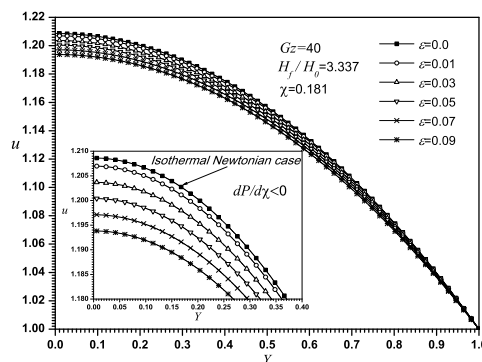


Fig. 5. Dimensionless velocity distribution u for different values of the parameter ϵ , as a function of the dimensionless transverse coordinate Y , evaluated at $\chi = 0.181$, for $H_f/H_0 = 3.337$ and $Gz = 40$.

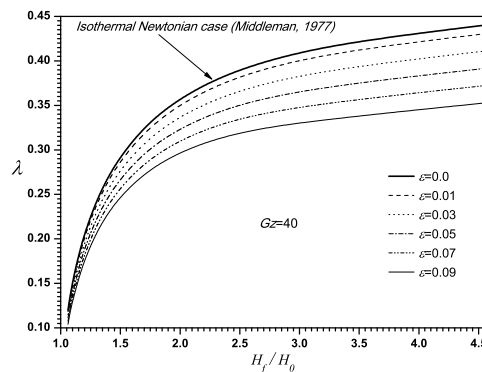


Fig. 6. The dimensionless leave-off distance λ as a function of the entering sheet thickness H_f/H_0 for different values of the parameter ϵ , for a Newtonian fluid with $Gz = 40$.

In Fig. 6 we show the complete result for the dimensionless leave-off distance, λ , as a function of the dimensionless entering sheet thickness, H_f/H_0 , under the influence of the parameters ϵ , for $Gz = 40$. In order to determine the correction λ_1 due to thermal effects, Eq. (50) was solved iteratively as a function of λ_0 , θ_0 and u_0 . The obtained results for λ_0 and λ_1 are replaced in the expansion of λ , given by $\lambda = \lambda_0 + \epsilon \lambda_1 + \dots$, for different values of the parameter ϵ . In this work, we have assumed that the rolls were fed with a sheet of fluid with finite thickness, as suggested in Fig. 1. In this case, the dimensionless entering sheet thickness H_f/H_0 is a known parameter as it is shown in Fig. 2. According to the above comments, the dimensionless entry distance, $-\chi_f$, is calculated following the relationship $\chi_f = (H_f/H_0 - 1)^{1/2}$. In all these figures, we can see that λ and H/H_0 increase for increasing values of H_f/H_0 , however λ and H/H_0 decrease for increasing values of ϵ . By comparison, in these figures we have included the case when no thermal effects are included ($\epsilon = 0$), which corresponds to the solution obtained by Middleman [8]. In these figures, for a fixed value of H_f/H_0 , the leave-off distance and the exiting sheet thickness decreases as the parameter ϵ increases. It is evident that non-isothermal Newtonian case produces thinner sheets than the isothermal Newtonian fluid. With the parametric values used in Figs. 9 and 10, the prediction of λ and H/H_0 show that these variables are strongly dependent on the assumed values of the parameter ϵ . For $H_f/H_0 = 4.54$ and $\epsilon = 0.09$, the leave-off distance

was reduced in about 20%, compared with the Newtonian isothermal case.

III. CONCLUSIONS

In this paper, we have studied theoretically the influence of the viscous dissipation and temperature-dependent consistency index on the exiting sheet thickness, for a Newtonian fluid flowing between two cylinders rotating at the same velocity and temperature. The solution is based on the regular perturbation technique and the resulting governing equations are based on the well-known Lubrication theory. The numerical results predict the dimensionless velocity field, pressure, temperature distribution, and the exit locations and the exiting sheet thickness corrected by thermal effects. A decrease of 20% in the in the leave-off distance was determined. As it has been shown, in the limit of $\epsilon \rightarrow 0$, the present solution smoothly approaches to the unperturbed or zeroth-order solution, corresponding just to the isothermal case previously reported by Middleman [8].

ACKNOWLEDGMENT

This work has been supported by the research grants no. 169849 of Consejo Nacional de Ciencia y Tecnología of Mexico and no. 20131535 of SIP-IPN.

REFERENCES

- [1] R. E. Gaskell, *The calendaring of plastic materials*, Journal of Applied Mechanics17, pp. 334-337.
- [2] J. M. McKelvey, *Polymer Processing*, Wiley, New York,1962
- [3] R. Zheng and R. I. Tanner, *A numerical analysis of calendaring*, Journal of Non-Newtonian Fluid Mechanics28, pp. 149170.
- [4] S. Sofou and E. Mitsoulis, *Calendaring of pseudoplastic and viscoplastic sheets of finite thickness*, Journal of Plastic Film Sheeting20, July, pp. 185–222.
- [5] E. Mitsoulis, *Numerical simulation of calendaring viscoplastic fluids*, Journal of Non-Newtonian Fluid Mechanics154 March, pp. 77–88.
- [6] F. Dobbels and J. Mewis, *Nonisothermal nip flow in calendaring operation*, AIChE Journal23(3), May, pp. 224–232
- [7] C. Kiparissides and J. Vlachopoulos, *A study of viscous dissipation in the calendaring of power-law fluids*, Polymer Engineering and Science18(3), pp. 210–214.
- [8] S. Middleman, *Fundamentals of Polymer Processing*McGraw-Hill, United States of America
- [9] Z. Tadmor and C. G. Gogos, *Principles of Polymer Processing*John Wiley Sons, Haifa, Israel
- [10] J. A. Dantzig and C. L. Tucker, *Modeling in Materials Processing*Addison-Wesley, Cambridge University Press

Creative Commons Attribution License 4.0 (Attribution 4.0 International, CC BY 4.0)

This article is published under the terms of the Creative Commons Attribution License 4.0
https://creativecommons.org/licenses/by/4.0/deed.en_US